

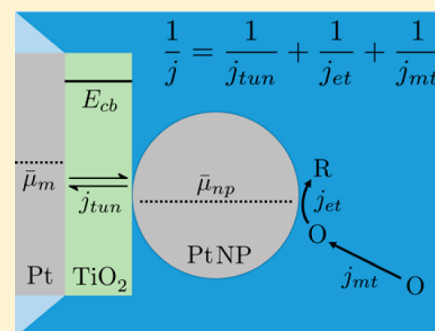
Electrochemistry at a Metal Nanoparticle on a Tunneling Film: A Steady-State Model of Current Densities at a Tunneling Ultramicroelectrode

Caleb M. Hill, Jiyeon Kim, and Allen J. Bard*

Center for Electrochemistry, Department of Chemistry, The University of Texas at Austin, Austin, Texas 78712, United States

S Supporting Information

ABSTRACT: Here, a new methodology is proposed for treating electrochemical current densities in metal-insulator-metal nanoparticle (M-I-MNP) systems. The described model provides broad, practical insights about MNP-mediated electron transfer to redox species in solution, where electron transfer from the underlying electrode to a MNP via tunneling and heterogeneous electron transfer from the MNP to redox species in solution are treated as sequential steps. Tunneling is treated through an adaptation of the Simmons model of tunneling in metal-insulator-metal structures, and explicit equations are provided for tunneling currents, which demonstrate the effect of various experimental parameters, such as insulator thickness and MNP size. Overall, a general approach is demonstrated for determining experimental conditions where tunneling will have a measurable impact on the electrochemistry of M-I-MNP systems.



1. INTRODUCTION

The electrochemical behavior of metal nanoparticles (MNPs) on a metal electrode (M) covered by an insulating film (I) sufficiently thin (~ 1 nm) so as to allow electronic communication through the film via tunneling is an area of recent interest. The addition of even a single MNP will effectively “reactivate” a M-I electrode, changing its behavior from passivated to electrochemically active with respect to a redox reaction in solution. Though several approaches have been explored to construct such M-I-MNP “tunneling electrodes”, by far the most widely studied have been organic monolayers deposited via self-assembly (self-assembled monolayers, or SAMs) or electrodeposition.^{1–3} Unfortunately, such films are not very rugged and almost all tend to have pinholes.

Using SAMs, Fermin^{4–7} and Gooding^{8–11} have shown that passivated electrodes can be reactivated by the attachment of MNPs onto the insulating SAM. This reactivation process is illustrated in Figure 1. In such an experiment, the long chain SAM layer largely suppresses the voltammetry of an outer-

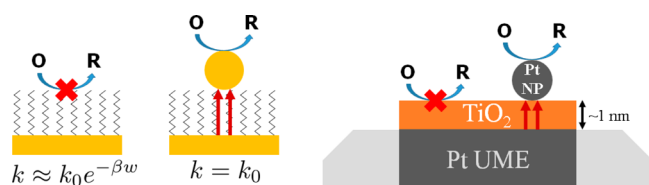


Figure 1. Reactivation of a passivated electrode through MNP adsorption (left) and schematic of the TUME system (right). O and R are chemical redox species involved in the generic electrochemical reaction $O + ne^- \rightarrow R$.

sphere reaction initially seen on the bare electrode. The attachment of MNPs on the SAM restores reversible electrochemistry at the electrode. Chazalviel and Allongue¹² provided an explanation of this behavior based on the much higher density of states (DOS) of the adsorbed MNPs as compared to those available on the redox species in solution, facilitating tunneling through the insulating film. Electrons can thus tunnel between the underlying bulk electrode and the adsorbed MNPs where the reaction takes place. At the MNP surface, as with any bare metal electrode, electrons only have to tunnel through a thin solvent layer which does not appreciably impact the measured kinetics.^{13,14} This reactivation effect has been observed not only with MNPs but also with semiconductor quantum dots,^{15–17} graphene,¹⁸ and carbon nanotubes.¹⁹

More recently, inorganic (e.g., metal oxide) layers have been investigated due to their comparatively higher physical and electrochemical stability. Metal oxide layers have been employed by our laboratory in the construction of tunneling ultramicroelectrodes (TUMEs),²⁰ where a single MNP is attached to an ultramicroelectrode (UME) passivated by a thin (~ 1 nm) TiO_2 film. The resulting TUME behaves effectively as a nanoelectrode with a geometry defined by that of the MNP. These TUMEs have many potential applications, including their use as probes in high resolution scanning electrochemical microscopy (SECM) or as nanoelectrodes for kinetic investigations. The construction of TUMEs may also provide a direct electrochemical means of investigating the reactivity of

Received: April 30, 2015

Published: August 17, 2015

individual MNPs or of characterizing the band structure of thin insulator/semiconductor films electrochemically.

Any of these potential applications demands a quantitative interpretation of the currents measured at a TUME. Proposed herein is a new, more quantitative model of electrochemistry at M-I-MNP electrodes such as the TUME. The model treats tunneling, heterogeneous electron transfer, and mass transfer as distinct, sequential steps with rates represented as steady-state current densities. The overall rate is then controlled by the slowest, rate-determining step, so the individual current densities add as shown in eq 1, which assumes a one electron transfer reduction of O to R with irreversible kinetics.

$$\frac{1}{j} = \frac{1}{j_{\text{tun}}} + \frac{1}{j_{\text{et}}} + \frac{1}{j_{\text{mt}}}$$

$$j_{\text{et}} = FC_{\text{O}}^* k^0 e^{-(\alpha F/RT)(E-E^0)} = FC_{\text{O}}^* k_{\text{f}}$$

$$j_{\text{mt}} = Fm_{\text{O}} C_{\text{O}}^* \quad (1)$$

Here, j is the total current density, F is the Faraday constant, m_{O} is the mass transfer coefficient, C_{O}^* is the concentration of the oxidized species O in bulk solution, k^0 is the standard rate constant, α is the transfer coefficient, R is the gas constant, T is the temperature, E is the applied potential, and E^0 is the formal potential for the reaction. j_{et} and j_{mt} are thus the limiting current densities which would result if the reaction were controlled solely by Butler–Volmer kinetics or mass transfer, respectively. This treatment is thus analogous to the Koutecký–Levich approach in rotating disk electrode voltammetry, with an additional j_{tun} term added to account for the effects of tunneling in the TUME system. In the present treatment, the current is considered to arise from a stepwise process: (1) tunneling from the underlying UME to the MNP, j_{tun} , which alters the electrochemical potential of electrons in the NP surface, j_{et} , and (3) mass transfer of the reactant, O, to the MNP surface, j_{mt} . The general case is outlined in the top panel of Figure 2. When a nonzero current is flowing, the electrochemical potentials of the UME and the MNP, $\bar{\mu}_{\text{m}}$ and $\bar{\mu}_{\text{np}}$, must be different in order to drive electron transfer across the insulating layer via tunneling. When the rate of tunneling through the insulating layer is low, as would be expected for a thick layer, $\bar{\mu}_{\text{np}}$ does not change appreciably from tunneling and remains pinned to the electrochemical potential of the redox couple in solution after the system reaches equilibrium. This limiting case, where j_{tun} is the limiting step, is depicted in the bottom-left panel of Figure 2 (Case T). When the tunneling is very fast, as would be expected for a thin insulating layer, $\bar{\mu}_{\text{np}} \approx \bar{\mu}_{\text{m}}$ and $j_{\text{et}}/j_{\text{mt}}$ becomes rate limiting. That is, the potential difference between $\bar{\mu}_{\text{m}}$ and $\bar{\mu}_{\text{np}}$ required to drive tunneling through the insulating film is negligible. This case is depicted in the bottom-right panel of Figure 2 (Case ET). This conceptual model for the electrochemical potentials of the UME, MNP, and redox species in solution is similar to that proposed recently by Scanlon et al.²¹ Experimentally, one would typically want to work in one of these two limiting regimes to study tunneling between the UME and MNP or electrochemistry at the MNP surface. Threshold values of experimental parameters (e.g., insulating layer thickness, redox species concentration) for these limiting cases would therefore have great utility and are derived in this paper.

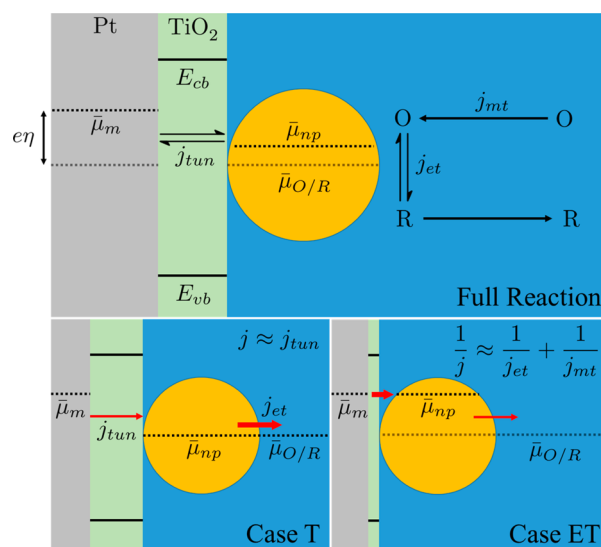


Figure 2. Schematic view of the consecutive processes involved in the TUME system, which result in the redox species, O, being reduced to R in solution (top). j_{tun} , j_{et} , and j_{mt} represent tunneling, electrochemical kinetic, and mass transfer controlled current densities, respectively. $\bar{\mu}$ represents electrochemical potentials (dotted lines) of the metal electrode, the NP, and the redox couple in solution. For a thick insulating layer, j_{tun} is small and $\bar{\mu}_{\text{np}} \approx \bar{\mu}_{\text{O/R}}$ (bottom left). For a thin layer, j_{tun} is large and $\bar{\mu}_{\text{np}} \approx \bar{\mu}_{\text{m}}$ (bottom right). In the bottom panels, the thicker red arrow denotes the faster process.

We first consider Case ET and a novel approach to treating the UME data, including a zone diagram that delineates control by electron transfer kinetics and by mass transfer. This is followed by a treatment of Case T, where tunneling is the rate-determining step, followed by zone diagrams for the full system.

2. RESULTS AND DISCUSSION

2.1. Case ET. Although this paper is concerned with the effect of tunneling to a MNP on the electrochemical response, it is instructive to start by considering only electron transfer at the MNP surface and mass transfer in solution as this demonstrates the general analytical approach with a well understood system. Novel experimental studies that utilize the approach outlined in this section to measure reaction kinetics will be published elsewhere.

If the tunneling step is very fast, $1/j_{\text{tun}} \rightarrow 0$ and, therefore, does not contribute appreciably in eq 1. The overall steady-state current density is then controlled solely by the electrochemical reaction as expressed below:

$$\frac{1}{j} = \frac{1}{j_{\text{mt}}} + \frac{1}{j_{\text{et}}} \quad (2)$$

Under these conditions, we want to understand the electrochemical behavior of the TUME in current–potential (I – E) space (voltammetry). In particular, we want to predict the effect of the applied potential, E , heterogeneous electron transfer kinetics, and mass transfer rates on measured currents in the TUME system. An important characteristic of the TUME is that its effective electrode geometry is determined by the geometry of the MNP, thus the mass transfer rate can be easily tuned by changing the size of the MNP used.

Consider the generic, one electron transfer reaction where a redox mediator, O, is irreversibly reduced to R at the MNP surface in a M-I-MNP system:

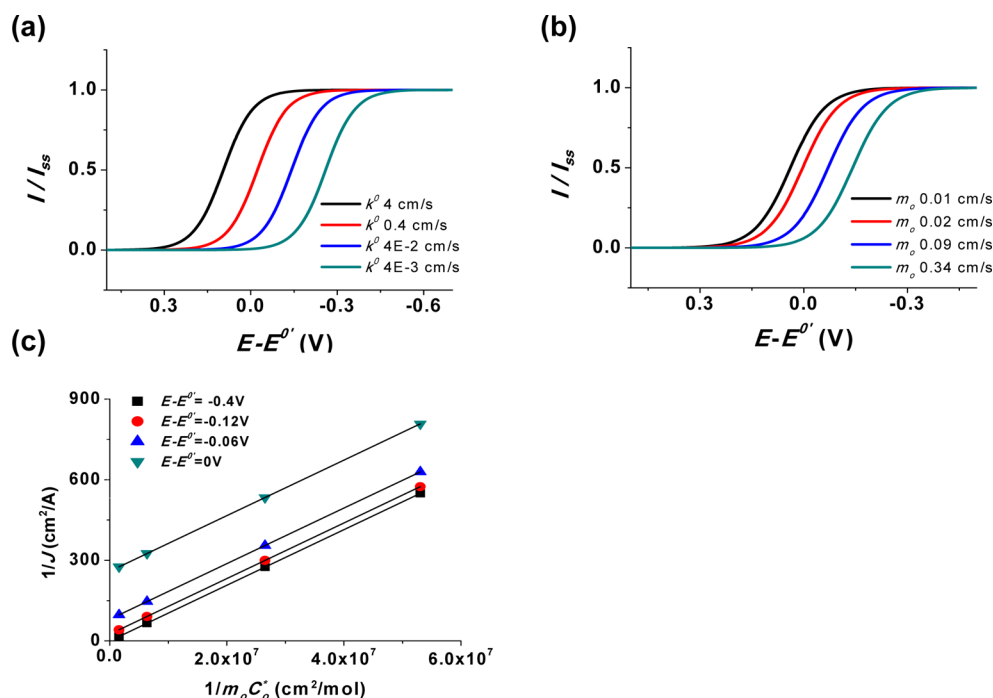


Figure 3. Case ET. (a) Normalized steady-state voltammograms simulated with $k^0 = 4, 0.4, 4 \times 10^{-2}$, and 4×10^{-3} cm/s at $m_O = 0.34$ cm/s ($r_0 = 0.15 \mu\text{m}$, $D = 7.4 \times 10^{-6}$ cm²/s). (b) Normalized steady-state voltammograms simulated with $m_O = 0.01, 0.02, 0.09$, and 0.34 cm/s at $k^0 = 4 \times 10^{-2}$ cm/s. In both (a) and (b), $\alpha = 0.5$. (c) A set of plots of $1/j$ vs $1/(m_O C_O^*)$ obtained from the voltammograms in (b) at $E - E^{0'} = 0, -0.06, -0.12$, and -0.40 V. At $E - E^{0'} = -0.40$ V, the reaction is mainly limited by mass transfer, thus, a plot of $1/j$ intersects the origin. Smaller values of $E - E^{0'}$ result in larger y -intercepts in the linear plots.



Here, we use the Butler–Volmer model to treat j ; thus, the current density equation for the irreversible ET reaction is written²² (see eqs S1–S4 in Supporting Information):

$$\frac{1}{j} = \frac{1}{j_{\text{mt}}} + \frac{1}{j_{\text{et}}} = \frac{1}{Fm_O C_O^*} + \frac{1}{FC_O^* k_f} \quad (4)$$

where $k_f = k^0 e^{-(\alpha F/RT)(E-E^{0'})}$. Equation 4 is analogous to the Koutecký–Levich treatment of rotating disk voltammetry, which includes contributions from both mass transfer and heterogeneous kinetics. Instead of varying the angular rotation rate of the electrode to alter mass transfer, the size of the UME (or the MNP in the TUME geometry) can be varied to alter the mass transfer coefficient, m_O , which can be expressed in terms of UME or MNP size and shape. For example, $m_O = 4D/\pi r_0$ for a disk UME and $m_O = (\ln 2)D/r_0$ for the TUME (modeled as a spherical electrode on an insulating plane) where r_0 is the radius of each geometry, which are well-known from the theory of UMEs.^{20,22}

As shown in Figure 3a, the I – E curve is a function of k^0 , shifting toward cathodic potentials with decreasing values of k^0 . Also, as the electrode radius decreases, mass transfer becomes more efficient and the current becomes more kinetically limited as well (Figure 3b). As depicted in Figure 3c, plotting $1/j$ vs $1/(m_O C_O^*)$ for various sizes of TUMEs (various values of m_O) should yield a linear plot with a slope of $1/F$. An extrapolation to $1/(m_O C_O^*) \rightarrow 0$ allows for the determination of the y -intercept, $1/FC_O^* k^0 e^{-(\alpha F/RT)(E-E^{0'})}$. Consequently, a series of such intercepts obtained at different overpotentials can be used to determine the kinetic parameters α and k^0 . To the authors'

knowledge, this approach has not been described previously in the literature and is useful for studying heterogeneous kinetics at all UMEs.

The ratio of ET current density to the mass transfer controlled current density, $j_{\text{et}}/j_{\text{mt}}$, will be taken as a measure of the kinetic limitation on the I – E curve and yields:

$$\frac{j_{\text{et}}}{j_{\text{mt}}} = \frac{k^0 e^{-(\alpha F/RT)(E-E^{0'})}}{m_O} = \frac{k_f}{m_O} \quad (5)$$

which is a function of m_O and k_f under a given $(E - E^{0'})$. The combined effects of k_f and m_O on the I – E behavior can be visualized in a 2-dimensional contour map analogous to a zone diagram, where $j_{\text{et}}/j_{\text{mt}}$ is plotted as a function of k_f and m_O . A plot of this type is given in Figure 4.

On the basis of this 2D map, we define the limiting zones empirically. For $k_f/m_O \geq 10$ (thus, $j_{\text{et}}/j_{\text{mt}} \geq 10$), j approaches j_{mt} even near $E^{0'}$ (upper dashed line in Figure 4). This condition is considered to define a mass transfer-controlled zone, MT. For $k_f/m_O \leq 0.1$ (thus, $j_{\text{et}}/j_{\text{mt}} \leq 0.1$), $j \approx j_{\text{et}}$ and kinetics dominates the current density resulting in a kinetically controlled regime, K (lower dashed line in Figure 4). The remaining region between $j \approx j_{\text{mt}}$ and $j \approx j_{\text{et}}$ (or $0.1 < j_{\text{et}}/j_{\text{mt}} < 10$) can be considered to be an intermediate zone, I, where j is heavily influenced by both mass transfer and kinetics. As kinetic information can be obtained either from either the intermediate zone, I, or kinetically controlled zone, K, it is important to know which combinations of k^0 , m_O , and $(E - E^{0'})$ are necessary for the desired kinetic study. Hence, these zone diagrams establish the range of measurable ET rate constants (k^0) for a given UME size and overpotential. The highest value

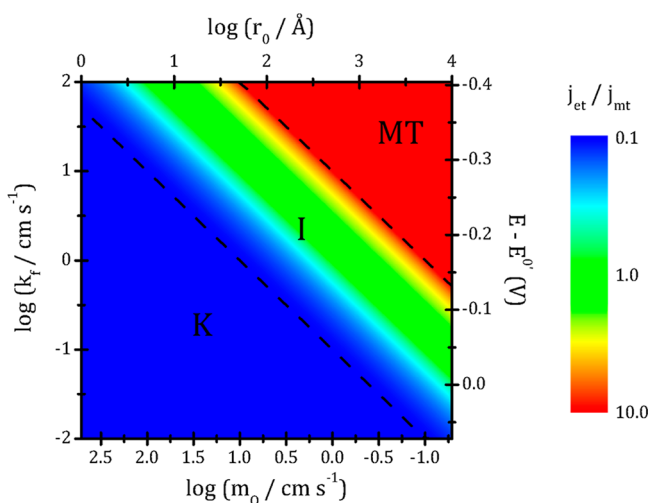


Figure 4. Ratio of kinetically controlled current density (j_{et}) to the mass transfer controlled current density (j_{mt}) as a function of k_f and m_0 , for a TUME system with $k^0 = 4 \times 10^{-2}$ cm/s and $D = 7.4 \times 10^{-6}$ cm²/s. When $j_{et}/j_{mt} \geq 10$ (i.e., $k_f/m_0 \geq 10$) (upper dashed line), the system is in a mass transfer controlled zone, MT. The zone where $j_{et}/j_{mt} \leq 0.1$ (i.e., $k_f/m_0 \leq 0.1$) (lower dashed line) represents a kinetically controlled zone, K. The remaining area is denoted as an intermediate zone, I.

of k_f/m_0 which can be determined using this approach is about 10, and a lower limit would be ~ 0.04 considering the magnitude of current densities which are reliably measurable. These limitations are in agreement with existing literature.^{23,24} In addition, the given zone diagram based on the spherical geometry of a TUME is applicable to a disk UME as well, since there is very little difference under irreversible conditions.^{25,26}

2.2. Case T. In the treatment of tunneling in the TUME system, a metal–insulator–metal (MIM) structure with the geometry depicted in Figure 5 is assumed. The system is

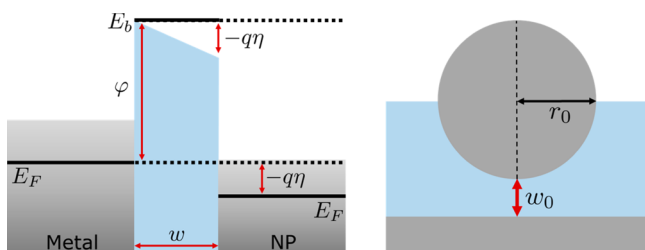


Figure 5. General schematic of MIM junction (left) and idealized geometry employed for calculating currents in a TUME system (right).

characterized completely by 4 parameters: ϕ , the offset between the Fermi level of the metal and the barrier potential (assumed to be the conduction band edge for a semiconductor layer), w_0 , the thickness of the tunneling barrier, r_0 , the MNP radius, and η , the potential difference between the UME and MNP. It is assumed that the UME and MNP are composed of the same metal. An adaptation of the Simmons²⁷ model for tunneling in planar MIM structures was derived and employed to treat tunneling in TUME structures. The interested reader is encouraged to consult the Supporting Information for a detailed discussion of the model employed. For brevity, only the important results will be given here.

At low overpotentials, the tunneling current density can be expressed as (see Supporting Information):

$$j_{\text{tun}} = -\frac{q^2 \eta}{8\pi h r_0^2} \left[\frac{w_0 + r_0}{w_0} \left(\frac{2a\phi^{1/2} w_0 + 0.486}{2a\phi^{1/2} w_0 + 1.451} \right) - 1 \right] e^{-2a\phi^{1/2} w_0} \quad (6)$$

where q is the elementary charge, h is the Planck constant, $a = (2m/\hbar^2)^{1/2} \approx 0.512$ eV^{-1/2} Å⁻¹, and the other terms are as defined above. This form of j_{tun} is linear in η and decreases exponentially with w_0 , as is typical in most treatments of tunneling. For large values of r_0 , it also varies inversely with r_0 .

Having established functional forms of j_{tun} , predicting whether a particular system would be under tunneling vs electrochemical control is straightforward. Since the smallest term in eq 1 will dominate, one needs only to compare the ratio of the tunneling and electrochemical current densities to make a useful prediction. When the electrochemistry is limited by mass transfer the ratio $j_{\text{tun}}/j_{\text{mt}}$ becomes:

$$\frac{j_{\text{tun}}}{j_{\text{mt}}} = -\frac{q^2 \eta}{8\pi \ln 2 F D C^* r_0 h} \left[\frac{w_0 + r_0}{w_0} \left(\frac{2a\phi^{1/2} w_0 + 0.486}{2a\phi^{1/2} w_0 + 1.451} \right) - 1 \right] e^{-2a\phi^{1/2} w_0} \quad (7)$$

Perhaps the most experimentally relevant quantity to predict is the tunneling layer thickness (w_0) at which the system will switch from electrochemical to tunneling control. Though no simple solution for w_0 in terms of a desired current density ratio can be easily written, the situation can be illustrated quite directly through plotting the current ratio as a function of w_0/r_0 . Such a plot is given in Figure 6. Contour lines for $j_{\text{tun}}/j_{\text{mt}} = 0.1$ and $j_{\text{tun}}/j_{\text{mt}} = 10$ are provided which designate the edge of the tunneling (T) and mass transfer (MT) controlled zones, respectively. Immediately obvious is that the current ratio is only weakly dependent on r_0 under diffusion controlled conditions, which is due to both j_{tun} and j_{mt} being inversely

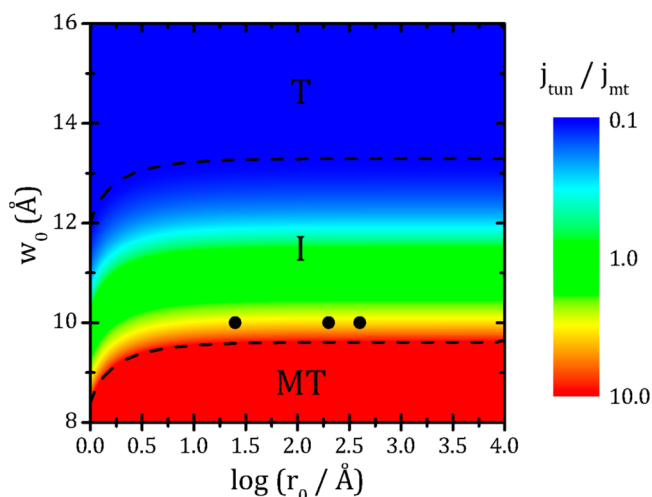


Figure 6. Ratio of tunneling and electrochemical (mass transfer-controlled) current densities as a function of w_0/r_0 for $\phi = 1.3$ eV, $\eta = -250$ mV, $D = 7.4 \times 10^{-6}$ cm² s⁻¹, and $C^* = 10$ mM. The dashed lines denote ratios of 0.1 and 10. Black circles designate w_0/r_0 combinations used by Kim et al.,²⁰ and the chosen experimental parameters reflect their experimental system. MT and T designate mass transfer controlled and tunneling controlled zones, respectively. I designates an intermediate zone.

proportional to r_0 . The critical dependence on w_0 due to the exponential factor in eq 6 is obvious, with the current ratio varying by a factor of 100 over a 5 Å range. This implies that clear experimental observation of the intermediate region would be extremely difficult to realize, as one would need to not only tune the average film thickness by subangstrom increments, but keep thickness variations in a $\sim 1 \mu\text{m}^2$ film to below 1 Å. In reality, within the tunneling film in a TUME there are regions that are above and below the threshold thickness for efficient tunneling. The relative electrode area capable of tunneling should then largely determine the functional properties of the film.

The previous experimental results of Kim and Bard with TUMEs are designated in Figure 6 by black dots, where the TiO_2 films used therein had an estimated thickness of 1 nm. On the basis of our calculations for these experimental systems, these experiments were carried out at the border between I and MT, which is consistent with their reported observation of mass transfer limited currents given the thickness variations discussed above.

Simple expressions for the current density ratio can be written for the kinetically limited case, as well. For totally irreversible kinetics, this ratio becomes:

$$\frac{j_{\text{tun}}}{j_{\text{et}}} = \frac{q^2 \eta}{8\pi F C^* r_0^2 k^0 h} \left[\frac{w_0 + r_0 \left(\frac{2a\varphi^{1/2} w_0 + 0.486}{2a\varphi^{1/2} w_0 + 1.451} \right) - 1}{e^{-2a\varphi^{1/2} w_0 + \alpha \eta}} - 1 \right] \quad (8)$$

Ratio values as a function of w_0/r_0 are plotted in Figure 7. The drastic dependence on w_0 is similar to the mass transfer-

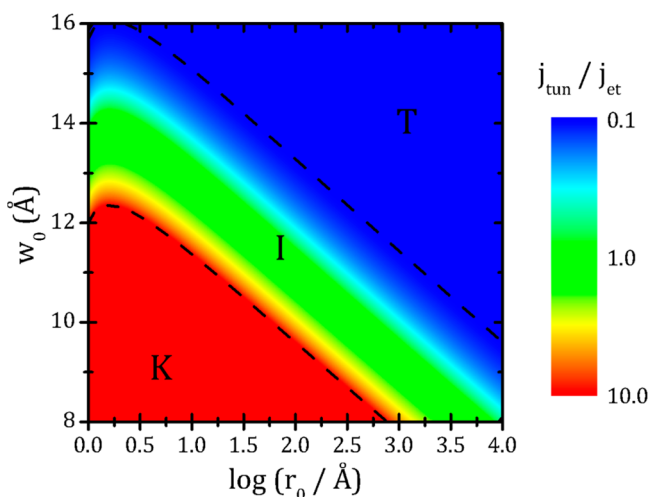


Figure 7. Ratio of tunneling and electrochemical (totally irreversible kinetics) current densities as a function of w_0/r_0 for $\varphi = 1.3$ eV, $\eta = -250$ mV, $k^0 = 0.04$ cm s⁻¹, and $C^* = 10$ mM. The dashed lines represent current density ratios of 0.1 and 10. Red and blue regions correspond to total electrochemical and tunneling control, respectively. K and T designate kinetically controlled and tunneling controlled zones, respectively. I designates an intermediate zone.

limited case. The dependence on r_0 , however, is much more significant, the ratio decreasing with increasing MNP size. This is due to j_{et} being independent of the size of the MNP.

In typical UME-MNP collision experiments, current steps due to MNP collisions are small even when limited only by mass transfer, on the order of 10–100 pA. When a TUME

experiment is tunneling controlled, the measured currents would then be even smaller. For example, if one is working within zone T in Figure 7, then $j \approx j_{\text{tun}} < 0.1 j_{\text{mt}}$ following eq 1. For practical purposes, such currents (1–10 pA or lower) may be undetectable. Due to the narrow intermediate region mentioned above, most MNP collisions would then be either detectable, with $j \approx j_{\text{mt}}$ or j_{et} , or undetectable. These situations would correspond to the red and blue regions, respectively, in Figures 6 and 7. An interesting exception to this argument would appear at large MNP sizes in the kinetically controlled case. Since both the tunneling and kinetic currents (not current densities) increase monotonically with r_0 , collisions of larger MNPs should always yield larger signals. Since this system is expected to be tunneling controlled at large r_0 , it is then feasible that MNPs above a certain size would be detectable with $j \approx j_{\text{tun}}$. This critical MNP size decreases with increasing tunneling layer thicknesses, which can be easily visualized in Figure 7.

Note that the zone diagrams given in Figures 6 and 7 would only be fully correct for rather extreme cases (i.e., for extremely large or small values of k_i/m_0). For realistic systems, the regions at small r_0 in Figure 6 and large r_0 in Figure 7 would fail. Correct results over the entire range of r_0 cannot be obtained without treating both mass transfer and kinetics. Such a treatment is depicted in Figure 8, which gives current densities

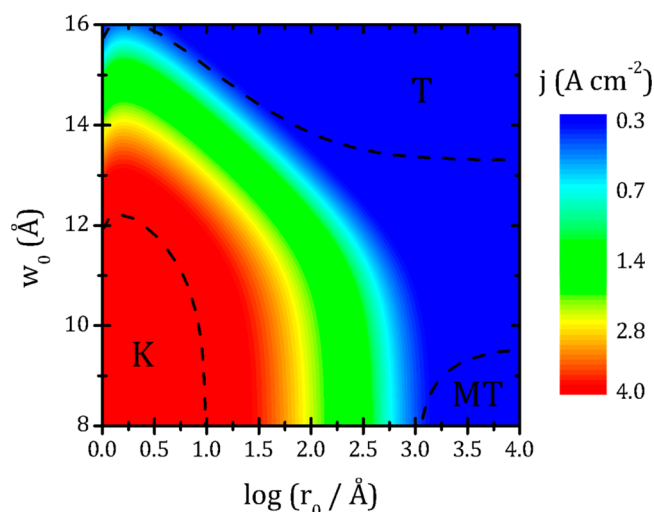


Figure 8. Current density in a TUME system calculated according to eq 1 as a function of w_0/r_0 for $\varphi = 1.3$ eV, $\eta = -250$ mV, $k^0 = 0.04$ cm s⁻¹, $D = 7.4 \times 10^{-6}$ cm² s⁻¹, and $C^* = 10$ mM. The dashed lines represent values of w_0/r_0 where the system crosses into tunneling, kinetic, or mass transfer control as defined in the text. Regions of tunneling, kinetic, and mass transfer control are denoted by T, K, and MT, respectively.

for an example TUME system calculated via eq 1, including the effects of tunneling, kinetics, and mass transfer. Zones where the current at the TUME is dominated by j_{tun} , j_{et} , or j_{mt} (T, K, or MT) are demarcated by dashed lines. This was defined in a manner similar to that employed in Figures 6 and 7 using the ratio of one component to the combination of the other two. For example, the boundary of zone T is defined by:

$$\frac{j_{\text{tun}}}{j_{\text{other}}} = j_{\text{tun}} \left(\frac{1}{j_{\text{other}}} \right) = j_{\text{tun}} \left(\frac{1}{j_{\text{et}}} + \frac{1}{j_{\text{mt}}} \right) = 0.1 \quad (9)$$

Zone diagrams such as these can be constructed easily using the relations provided in this report for any desired TUME (or other M-I-MNP) system, and can serve as a valuable tool in future experimental work.

3. CONCLUSIONS

A steady-state approach to treating currents in the TUME system has been developed which treats tunneling between a UME and MNP, heterogeneous electron transfer at the MNP surface, and mass transfer of redox species in solution as independent, sequential steps. A simple analytical expression for the tunneling current density in the TUME system was given based on an adaptation of the Simmons model to the M-I-MNP geometry. Mass transfer and heterogeneous kinetics at the MNP surface, treated through the Butler–Volmer model, were treated as competing pathways for the following electrochemical process. Expressions for tunneling and electrochemical current densities were used to predict whether a particular TUME system would fall under tunneling or electrochemical control. For mass transfer controlled electrochemistry, the crossover between tunneling and electrochemical control is predicted to occur abruptly at film thicknesses in the range of 1 to 2 nm, while it is relatively insensitive to the MNP radius. These predictions agree with the previous report of Kim and Bard, where total electrochemical control was observed for ~1 nm TiO₂ films with MNPs between 5 and 80 nm in diameter. For electrochemistry controlled by heterogeneous kinetics, the dependence on film thickness is similar to the mass transfer controlled case, while the MNP size exhibits a much greater effect, the system becoming more tunneling controlled with increasing MNP size. Zone diagrams outlining combinations of film thicknesses and particle sizes, which result in tunneling, kinetic, and mass transfer control, were also given. The straightforward treatment provided here can be readily applied to future experiments with TUMEs and related M-I-MNP systems.

■ ASSOCIATED CONTENT

● Supporting Information

The Supporting Information is available free of charge on the ACS Publications website at DOI: 10.1021/jacs.5b04519.

Detailed derivations and discussion of the tunneling model employed for the TUME system (PDF)

■ AUTHOR INFORMATION

Corresponding Author

*ajbard@mail.utexas.edu

Notes

The authors declare no competing financial interest.

■ ACKNOWLEDGMENTS

The authors thank J.-N. Chazalviel and Marshall Newton for providing their valuable input on the manuscript. C.M.H. would also like to acknowledge J. E. Dick and C. Renault for helpful discussions. We acknowledge support of this research from the AFOSR MURI (FA9550-14-1-0003) and the Robert A. Welch Foundation (F-0021).

■ REFERENCES

- (1) Love, J. C.; Estroff, L. A.; Kriebel, J. K.; Nuzzo, R. G.; Whitesides, G. M. *Chem. Rev.* **2005**, *105*, 1103–1170.
- (2) Daniel, M.-C.; Astruc, D. *Chem. Rev.* **2004**, *104*, 293–346.

- (3) Barfidokht, A.; Ciampi, S.; Luais, E.; Darwish, N.; Gooding, J. J. *Anal. Chem.* **2013**, *85*, 1073–1080.
- (4) Zhao, J.; Bradbury, C. R.; Huclova, S.; Potapova, I.; Carrara, M.; Fermin, D. J. *J. Phys. Chem. B* **2005**, *109*, 22985–22994.
- (5) Zhao, J.; Bradbury, C. R.; Fermin, D. J. *J. Phys. Chem. C* **2008**, *112*, 6832–6841.
- (6) Kissling, G. P.; Miles, D. O.; Fermin, D. *Phys. Chem. Chem. Phys.* **2011**, *13*, 21175–21185.
- (7) Bradbury, C. R.; Zhao, J.; Fermin, D. J. *J. Phys. Chem. C* **2008**, *112*, 10153–10160.
- (8) Barfidokht, A.; Ciampi, S.; Luais, E.; Darwish, N.; Gooding, J. J. *Anal. Chem.* **2013**, *85*, 1073–1080.
- (9) Shein, J. B.; Lai, L. M. H.; Eggers, P. K.; Paddon-Row, M. N.; Gooding, J. J. *Langmuir* **2009**, *25*, 11121–11128.
- (10) Liu, G.; Luais, E.; Gooding, J. J. *Langmuir* **2011**, *27*, 4176–4183.
- (11) Dyne, J.; Lin, Y.-S.; Lai, L. M. H.; Ginges, J. Z.; Luais, E.; Peterson, J. R.; Goon, I. Y.; Amal, R.; Gooding, J. *ChemPhysChem* **2010**, *11*, 2807–2813.
- (12) Chazalviel, J.; Allongue, P. *J. Am. Chem. Soc.* **2011**, *133*, 762–764.
- (13) Marcus, R. J. *Chem. Phys.* **1956**, *24*, 966–978.
- (14) Khairutdinov, R. F.; Zamaraev, K. I.; Zhadanov, V. P. *Electron Tunneling in Chemistry*; Elsevier: New York, 1989; Vol. 30.
- (15) Kissling, G. P.; Bünzli, C.; Fermin, D. J. *J. Am. Chem. Soc.* **2010**, *132*, 16855–16861.
- (16) Vanmaekelbergh, D.; Liljeroth, P. *Chem. Soc. Rev.* **2005**, *34*, 299–312.
- (17) Bakkers, E.; Roest, A. L.; Marsman, A. W.; Jennekens, L. W.; de Jong-van Steensel, L. I.; Kelly, J. J.; Anmaekelbergh, D. *J. Phys. Chem. B* **2000**, *104*, 7266–7272.
- (18) Zhang, B.; Fan, L.; Zhong, H.; Liu, Y.; Chen, S. *J. Am. Chem. Soc.* **2013**, *135*, 10073–10080.
- (19) Dumitrescu, I.; Unwin, P. R.; Macpherson, J. V. *Chem. Commun.* **2009**, 6886–6901.
- (20) Kim, J.; Kim, B.-K.; Cho, S. K.; Bard, A. J. *J. Am. Chem. Soc.* **2014**, *136*, 8173–8176.
- (21) Scanlon, M.; Peljo, P.; Mendez, M. A.; Smirnov, E.; Girault, H. H. *Chemical Science* **2015**, *6*, 2705–2720.
- (22) Bard, A. J.; Faulkner, L. R. *Electrochemical Methods, Fundamentals and Applications*, 2nd ed.; John Wiley & Sons: New York, 2001.
- (23) Oldham, K. B.; Myland, J. C.; Zoski, C. G.; Bond, A. M. *J. Electroanal. Chem. Interfacial Electrochem.* **1989**, *270*, 79–101.
- (24) Mirkin, M. V.; Bard, A. J. *Anal. Chem.* **1992**, *64*, 2293–2302.
- (25) Bond, A. M.; Oldham, K. B.; Zoski, C. *Anal. Chim. Acta* **1989**, *216*, 177–230.
- (26) Oldham, K. B.; Zoski, C. J. *Electroanal. Chem. Interfacial Electrochem.* **1988**, *256*, 11–19.
- (27) Simmons, J. G. *J. Appl. Phys.* **1963**, *34*, 1793.